EES Catalysis

PAPER

Check for updates

Three-in-one approach to fabricate a porous porphyrin-heptazine polymer for highly efficient visible light photocatalysis†

Weijie Zhang,‡[a] Zhou Lu, [ID] ‡[a] Dipesh Adhikari,[b] Shan Li, [ID] [a] Thamraa AlShahrani [ID] [c] and Shengqian Ma [ID] *[a]

Efficient metal-free heterogeneous photocatalysts, using visible light from the sun, continue to be a design challenge for use in chemical synthesis. Compared to metal-free photocatalysts involving a fundamental redox process, multi-dimensional photocatalytic systems with enhanced performance are limited. In this contribution, we demonstrated a general three-in-one approach to construct a donor–acceptor (D–A)-based porous organic polymer *via* connecting the most applied porphyrin with heptazine into a porous framework structure. Herein, a cooperative excitation process for O_2 activation was established, where porous organic polymers can not only generate $^1O_2$ under light irradiation *via* a triplet state, but also capture O_2 and reduce it to $O_2^{\bullet-}$. This synergistic effect dramatically improved the photocatalytic performance, as exemplified in the context of several important aerobic oxidative transformations, including sulfur mustard simulant degradation, oxidative coupling of primary amine molecules, and oxidative conversion of sulfides. Our work, therefore, paves a new way for the development of highly efficient heterogeneous photocatalysts.

Broader context

Solar energy, a clean and abundant resource for synthesizing chemicals, has become a major objective in green chemistry. One issue that has plagued the practical applications of many efficient catalytic systems is their low stability and single cycle use in homogeneous or heterogeneous systems. Therefore, designing efficient, inexpensive, recyclable heterogeneous metal-free photocatalysts will promote environmentally cleaner methods for synthesizing valuable materials. In this work, we contribute a general and effective approach for exploring highly efficient heterogeneous photocatalysts by constructing a photoactive donor–acceptor (D–A) porous organic polymer. When the two components are connected into a porous organic polymer, a photo-catalytically favored three-in-one process is established, which leads to dramatic improvement of photocatalytic performances.

Introduction

Typically, light-driven oxidative/reductive (redox) processes are limited in semiconductor assemblies, among which electron transfer has been conducted as the primary photo-induced reductive pathway on a single site.[1] In order to incorporate the proper energetics for charge accumulation and separation, some building block molecules, such as porphyrin, perylene, and pyrene, have been employed to combine electron and energy transfer events in supramolecular assemblies.[2] In particular, the advancements of photo-induced electron and energy transfer in a donor–acceptor (D–A) heterojunction facilitate the development of efficient light-harvesting systems.[3,4]

Similarly, the activation of O_2 in an ecological manner occurs by two separate mechanisms: (I) stepwise monovalent reduction *via* an electron-transfer process where O_2 is reduced to $O_2^{\bullet-}$, which can be further disproportionated to form $HO^{\bullet}$ and H_2O_2, and (II) energy transfer to reverse the spin on one of the unpaired electrons such that $^1O_2$ is sequentially formed (as shown in Scheme S1, ESI†). The activation of O_2 is challenging in diverse contexts, ranging from biology to material dissolution. Relatively high oxygen pressure ($\sim$5 atm), temperature ($\sim$373 K), and/or long-lived *N*-oxyl radicals such as TEMPO are

[a] Department of Chemistry, University of North Texas, Denton, TX 76203, USA.
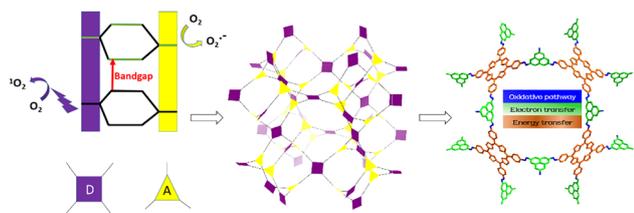E-mail: Shengqian.Ma@unt.edu

[b] Department of Chemical Engineering, University of Virginia, Charlottesville, VA 22903, USA

[c] Department of Physics, College of Science, Princess Nourah bint Abdulrahman University, Riyadh 11564, Saudi Arabia

‡ These two authors contributed equally to this work.

Scheme 1 Schematic representation of the donor–acceptor PHP for the proposed three-in-one photocatalysis.

usually required.[5] As such, we postulate that a three-in-one D–A system photocatalyst designed to include an efficient oxidative pathway, electron transfer, and energy transfer processes will boost the activation of O_2 in a multi-dimensional photocatalytic system.

Conjugated microporous polymers (CMPs),[6–17] a group of organic porous polymers that combine π-conjugated skeletons with permanent porosity, thermal/chemical stability, high surface area, and structural flexibility, provide a great platform for discovering and designing efficient photocatalysts. CMPs are particularly appealing as they are fine-tunable at the molecular level, allowing for the study of structure–property relationships of the polymers in detail.[18–20] Many studies have focused on CMP photocatalysts with favourable energy band positions for stable and efficient organic synthesis.[21–25] Recently, a significant increase in photocatalytic efficiency was achieved by fabricating CMPs through a copolymerization reaction to join donor (D) and acceptor (A) molecules.[26,27]

Bearing the above in mind, we selected two most applied materials in a controlled manner to synergize their properties in the CMP-based D–A system as photocatalysts. Firstly, to improve the light-harvesting abilities of the material, we selected porphyrin molecules because they possess a high molar absorptivity and can be custom-designed to target porous materials.[28] Porphyrin molecules have been widely utilized as sensitizers due to their long excited state lifetimes in energy transfer processes.[29–32] In addition, porphyrin dyes are photoactive electron-donors, which benefits the D–A system.[33] Secondly, graphitic carbon nitride (g-C_3N_4), as a metal-free photocatalyst, has been adopted, consisting of heptazine units in a layered structure connected at the vertices through amino groups and being demonstrated to be capable of oxidizing amines into imines irradiated by visible light.[34] Structurally, such a robust 3D cage-like ultra-microporous network by [4+3] condensation would result in a high Brunauer–Emmett–Teller (BET) specific surface area as well as good thermal and physicochemical stability. We hypothesize that the combined synergy from heptazine and porphyrin incorporated into the π-conjugated framework will afford an exclusive heterogeneous photocatalytic system benefiting the aforementioned three-in-one approach (Scheme 1).

Results and discussion

To demonstrate this proof-of-concept, we started from meso-tetra(4-nitrophenyl)porphyrin (TNPP) and heptazine to obtain

an azo-linked[35,36] porous organic polymer in yields up to 63% (ESI†). N_2 sorption isotherms collected at 77 K (Fig. 1a) on the porphyrin-heptazine polymer (PHP) recorded a calculated Brunauer–Emmett–Teller (BET) surface area of ~ 465 m^2 g^{-1} (Langmuir surface area ~ 707 m^2 g^{-1}) and exhibited hysteresis between the adsorption and desorption isotherms. This type of isotherm occurs when a hierarchical porous structure comprising both micropores and mesopores was present as shown in the pore size distribution (Fig. S1, ESI†). The chemical composition of PHP was further confirmed by solid-state ^{13}C NMR (Fig. 1b) and ^{15}N NMR (Fig. S2, ESI†) spectral analysis.

Transmission electron microscopy (TEM) images of PHP were interpreted to show that PHP is composed of interconnected porous nanosheets (Fig. S3, ESI†). The wider field viewed from scanning electron microscopy (SEM) witnessed a tight network-like structure (Fig. S4, ESI†). The thermal gravimetric (TG) analysis revealed that PHP has no obvious weight loss, besides adsorbed water, before complete carbonization beginning at 350 °C (Fig. S5, ESI†). The optical properties of PHP were examined using UV-Vis diffuse reflectance spectroscopy. As shown in Fig. S6 (ESI†), the purple PHP can absorb light over the visible spectrum. Compared to TNPP, PHP is red-shifted by 9 nm, thus confirming bonding between TNPP and heptazine moieties. The absorption band edge of PHP at 687 nm has an optical bandgap value of 1.80 eV.

Reducing the contamination impact of chemical warfare agents (CWAs) is a vital issue.[37] As one representative of CWAs, sulphur mustard is usually detoxified by the selective oxidation strategy. Thus, it is highly desired to design catalysts that can catalytically degrade sulphur mustard. In the lab, 2-chloroethyl ethyl sulphide (CEES) is an effective sulphur mustard simulant
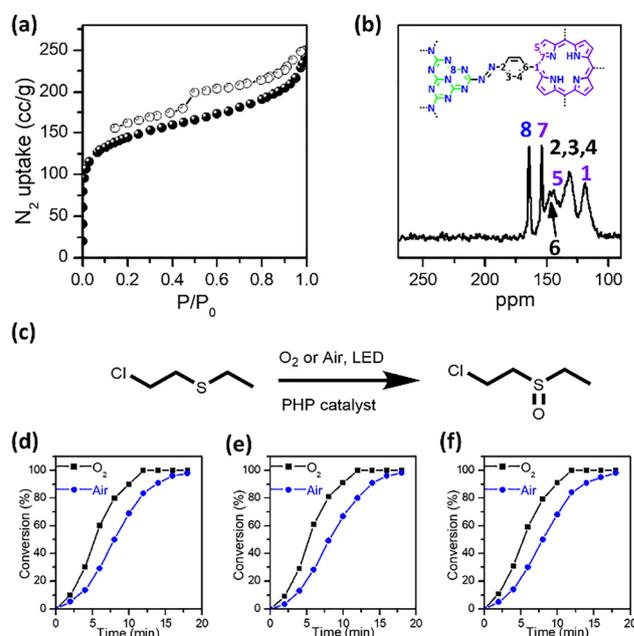

Fig. 1 (a) The N_2 adsorption and desorption isotherms of PHP tested at 77 K; (b) solid-state ^{13}C CP/MAS NMR spectra of PHP; (c)–(f) photooxidation of CEES under LED irradiation and O_2 atmosphere catalyzed by PHP.

and will be used for our study. Among most reported cases, either hydrogen peroxide (H_2O_2) or *tert*-butyl hydroperoxide (*t*-BuOOH) has been employed as an oxidant. However, because of their powerful oxidizing ability, it remains challenging to modulate the two oxidation products: 2-chloroethyl ethyl sulfoxide (CEESO, target product) and 2-chloroethyl ethyl sulfone (CEESO$_2$, by-product). Prominent among extensive efforts that have been undertaken for the oxidation of sulphides into sulfoxides is O_2 utilization under mild conditions.[37–39] It is imperative to selectively oxidize CEES into CEESO without the possible CEESO$_2$ generated, particularly using a mild photo-oxidation method, mainly due to the high toxicity of CEESO$_2$.

In this strategy, PHP was employed as a photosensitizer to generate $^1O_2$ upon LED irradiation. The CEES oxidation in the presence of PHP under O_2 is illustrated in Fig. 1c. To perform the oxidation, PHP (0.5 mol%) was suspended in the solvent and then sealed in a glass tube before purging O_2. CEES was then introduced, and the reaction mixture was monitored by GC-MS (Fig. S7 and S8, ESI†), ^1H NMR (Fig. S9, ESI†), and ^{13}C NMR (Fig. S10, ESI†). As shown, almost no by-product (CEESO$_2$) was evident, with a full conversion after 12 min. Fig. 1c–f establishes the kinetic aspects of the oxidation reaction, for three consecutive injections of CEES into the same reaction irradiated by LED light. The full conversion of the second and third aliquots demonstrated the reusability of the PHP catalyst. For comparison, at 0 min, ^{13}C NMR peaks at 43, 34, 26, and 15 ppm showed the presence of the mustard gas simulant CEES (Fig. S10, ESI†). After 12 min, these peaks disappeared, and new peaks were then observed at 53, 45, 36, and 6 ppm, indicating full transformation of CEES into CEESO. Furthermore, an additional catalyst stability test revealed that the conversion remains 100% for 5 cycles with no obvious activity decay (Fig. S11, ESI†). This result demonstrated that $^1O_2$ can be easily generated by PHP upon irradiation with a commercially available LED source.

Moreover, aromatic sulfoxide compounds play a crucial role as intermediates in organic synthesis or as bioactive compounds in the pharmaceutical industry.[40] To further determine the photocatalytic efficiency of PHP, selective photo-oxidation of aromatic sulphides was conducted under the same conditions using visible-light irradiation and O_2 as an oxidant. As depicted in Table S1 (ESI†), it is demonstrated that PHP can catalyse the conversion of a wide range of sulphides into sulfoxides with remarkable efficiency and high selectivity.

To gain further insight into the three-in-one mechanism, the oxidative coupling of aromatic amines has been selected as the model reaction to investigate the oxidative pathway, electron transfer, and energy transfer processes. This reaction has an essential role in the design and construction of highly valuable building blocks for pharmaceutical applications.[40] However, traditional methods have persistent problems such as poor selectivity, low efficiency, and the requirement of harsh reaction conditions. These prerequisites hamper their widespread applications. A recent report utilized photo-heterogeneous catalysts and O_2 as an oxidant for imine production.[41] In our approach, we also tested PHP as a visible-light photocatalyst for the oxidative coupling reaction of benzylamine (BA) under 1 atm of O_2 at 25 °C.

In the absence of light, PHP showed no activity to convert BA into *N*-benzylidenebenzylamine after three hours (entry 1, Table S2, ESI†). Similarly, the reaction cannot proceed without PHP irradiated by visible light only (entry 2, Table S2, ESI†). Control experiments were also carried out for heptazine, TNPP, and g-C$_3$N$_4$ under identical conditions. As shown in Fig. S12 (ESI†), after three hours of irradiation, PHP displayed the highest catalytic activity for the benzylamine oxidative coupling (>99% after 3 h). This compared favourably to the corresponding conversion for free base TNPP (27%), g-C$_3$N$_4$ (13%), and heptazine (10%) (entries 3–5, Table S2, ESI†). This dramatic enhancement in the catalytic performance of PHP is ascribed to the synergistic effect of heptazine moieties and porphyrin units, which are interconnected throughout the highly porous framework structure. The supernatant after filtration did not afford any other oxidation products, confirming the heterogeneous and robust nature of the PHP catalyst (Fig. S13, ESI†). Upon completion of the reaction, the simple filtration led to nearly quantitative recovery of PHP without a significant drop in its reactivity (Fig. S14, ESI†). Importantly, all the photocatalytic reactions tested in this study achieved high selectivity.

High conversion and excellent selectivity were observed when various amine molecules were screened using PHP to assess the electronic effect on the coupling reactions (entries 9–13, Table S2, ESI†). These outstanding results can presumably be attributed to the high density of accessible active sites in the hierarchical porous structure of PHP, which facilitates the mass transport, thereby assisting high yields in a relatively short period of time. It must be noted that a physical mixture of porphyrin and heptazine showed almost no activity enhancement, suggesting that the covalent interaction of porphyrin with heptazine is necessary.

To gain insights into the above coupling reactions promoted by PHP, a series of thermodynamic and kinetic studies were performed to understand the underlying mechanisms of the photo-redox processes. For the redox coupling reactions to proceed under visible irradiation, the photocatalyst bandgap is required to be close in energy potential to product formation. To estimate the relative positions of the conduction band (CB) and the valence band (VB) edges, electrochemical Mott–Schottky experiments were carried out (Fig. 2a). The positive slope of the plot indicated that PHP is a classical n-type semiconductor. From the *x*-intercept, the CB minimum was determined to be −0.36 V *versus* Ag/AgCl at pH ∼ 6.6. This result, together with the bandgap energy, enabled us to determine the VB edge at ∼1.44 V (Fig. 2b). The CB edge of PHP was lower compared with g-C$_3$N$_4$, with ∼0.89 V downshift from −1.25 to −0.36 V. These results demonstrated that the incorporation of photoactive electron-donating porphyrin can greatly reduce the CB level of the composite, thereby increasing the photo-reduction capability. Taken together, these findings clearly established that PHP has a suitable band structure with a CB level of high photo-reduction capability and a VB level that efficiently facilitates BA oxidation.

To elaborate on the three-in-one mechanism of the photocatalytic reaction and the crucial roles of the photo-generated hole–electron pairs upon oxidative coupling reactions of benzylamines,
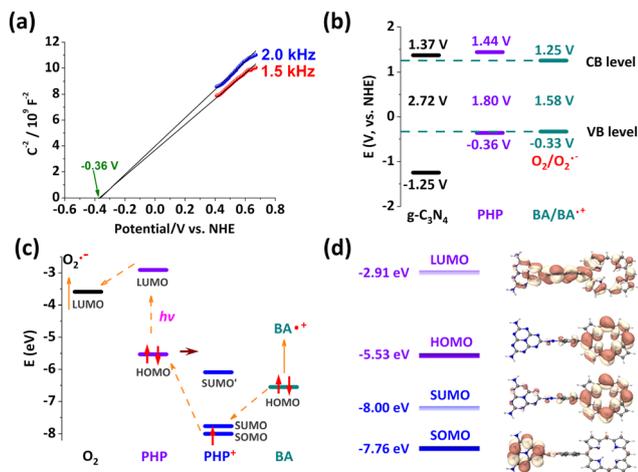
Fig. 2 (a) Mott–Schottky plot of sample PHP at 1.5 (red) and 2.0 kHz (blue). (b) Comparison of the band gap of g-C$_3$N$_4$,[42] PHP determined in this work, the redox potential of O$_2$/O$_2$$^{\bullet-}$ (−0.33 eV)[43] and the redox potential of BA/BA$^{\bullet+}$ (BA = benzylamine).[44] (c) Calculated energy level diagram and mechanism of the fundamental photoredox process. (d) Contours of frontier molecular orbitals of PHP and PHP$^+$ with isovalues of 0.02 a.u.
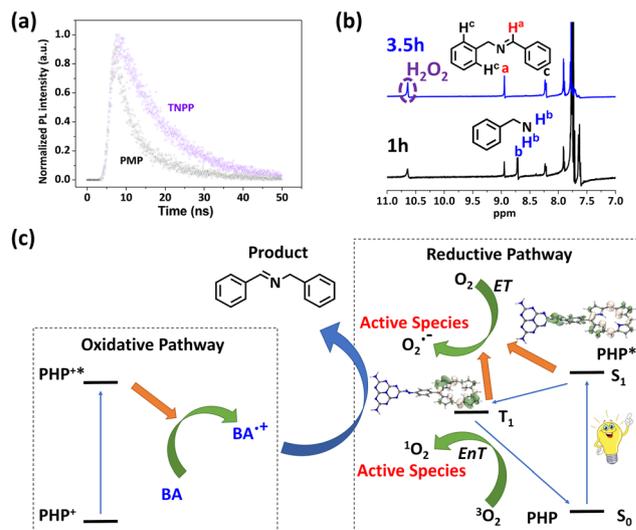

Fig. 3 (a) Time-resolved PL kinetics for TNPP (purple point) and PHP (black point), recorded with excitation at 420 nm and emission at 712 nm. (b) ^{1}H NMR spectra of the reaction mixture after 1 hour (black) and 3.5 hours (blue), showing the formation of H$_2$O$_2$ and the imine product. (c) Proposed three-in-one reaction mechanism combining oxidative and reductive pathways. Inset figures are electron density difference (EDD) maps of the corresponding excited states of PHP with an isovalue of 0.0005 a.u. BA: benzylamine; ET: electron transfer; EnT: energy transfer.

thermodynamic information about the energy levels were calculated on a porphyrin-heptazine model (Fig. 2c). Since the state of the cationic PHP (PHP$^+$, formed during the photocatalytic cycles after electron being transferred to oxygen) is in a doublet spin state, we defined that the singly unoccupied molecular orbital (SUMO) and the singly occupied molecular orbital (SOMO) are the lowest unoccupied beta orbital and the highest occupied beta orbital, respectively. The energy level of the LUMO of PHP was higher than that of oxygen, thus leading to catalytically active oxygen radical species O$_2$$^{\bullet-}$ (superoxide anion). The HOMO energy level of BA was higher than the SOMO of PHP$^+$ (Fig. 2c). Therefore, holes can provide a sufficient thermodynamic driving force to oxidize the BA. Given these findings, it can be concluded that the photo-redox pathway for the oxidative coupling of BA by PHP is completely achievable and most likely to follow an oxidative quenching process, as illustrated in Scheme S2 (ESI†).[43]

Next, we investigated the photoluminescence (PL) response to confirm photo-induced hole transfer from PHP to BA (Fig. S15 and S16, ESI†). PL quenching after bubbling O$_2$ occurred due to the triplet–triplet annihilation (TTA) with photoexcited ^{3}PHP* (Fig. S16, ESI†). This reductive quenching of PHP could cause the oxidation of BA to yield a BA radical cation, as previously reported.[43] Accordingly, the PHP exhibited considerably enhanced constant photocurrent, which was almost three times greater than that of pristine g-C$_3$N$_4$, indicating that more electrons can be photo-generated and then transferred (Fig. S17, ESI†). It is assumed that the incorporation of porphyrin renders the composite with an increased capacity for light adsorption, and the presence of heptazine facilitates the hole–electron separation and transportation during the photocatalytic process, which is direct evidence to support the proposed mechanism, as shown in Scheme S2 (ESI†).

PL emission quenching is in line with catalysts displaying a higher photocatalytic activity.[45] Notably, the steady-state PL

measurement (Fig. S18, ESI†) displayed a significant PL emission quenching, suggesting a greatly suppressed radiative hole–electron recombination in PHP compared to TNPP. To elucidate the kinetics of the trap state, the time-resolved PL technique was conducted to find the emission lifetimes of 12.07 ± 0.03 and 5.94 ± 0.03 ns for TNPP and PHP at 712 nm (Fig. 3a), respectively. The shorter PL lifetime arises from rapid charge transfer between the donor (porphyrin) and acceptor (heptazine) units, which quenches exciton emission in favor of generating long-lived charges. Therefore, the enhanced photocurrent and quenched PL together result in enhanced photocatalytic performance for the PHP material.[45]

Superoxide radicals have been previously reported to abstract one hydrogen atom at the benzylic position of the BA radical cation, thereby forming benzylimine and the by-product hydrogen peroxide in a 1 : 1 ratio.[46] Therefore, the reaction mixture of BA coupling was monitored by ^{1}H NMR spectroscopy to observe the formation of H$_2$O$_2$ at 10.95 ppm (Fig. 3b and Fig. S19, ESI†). The integrated peak areas between H$_2$O$_2$ and benzenemethanamine were found with a ratio of 1 : 1.4. From this result, we concluded that the oxidative coupling reaction follows both the expected energy transfer and electron transfer pathways, whereas the latter one was the predominant mechanism.

To kinetically monitor electron transfer from BA to O$_2$ promoted by PHP, 1,4-bis(dimethylamino)benzene was used as an indicator molecule to track the superoxide radical (O$_2$$^{\bullet-}$) formation.[45] The electron transfer from the 1,4-bis(dimethylamino)benzene to dioxygen gave rise to the formation of a cationic radical complex in blue colour (Fig. S20, ESI†). As shown in Fig. S21 (ESI†), the photocatalytic properties associated with

the generation of singlet oxygen ($^1O_2$) upon irradiation of PHP were explored using 1,3-diphenylisobenzofuran (DPBF).[47] Through the electron density difference (EDD) map of PHP in the T_1 state, the TNPP unit mainly contributed to the electron excitation (Fig. 3c). However, time-dependent absorbance decay of DPBF revealed a fast consumption upon $^1O_2$ in the presence of PHP, while a slower decay was observed in the presence of TNPP only, suggesting lower photoactivity (Fig. S22, ESI†). This result highlighted that the incorporation of the porphyrin and heptazine moieties promoted the reactivity.

Similar results were observed in spin trap electron paramagnetic resonance (EPR) experimental results using 2,2,6,6-tetramethylpiperidinyloxyl (TEMPO) and 5,5-dimethyl-1-pyrroline N-oxide (DMPO) as $^1O_2$ and $O_2^{\bullet-}$ trapping agents, respectively. As shown in Fig. S23 and S24 (ESI†), both catalytically active oxygen radical species $O_2^{\bullet-}$ and $^1O_2$ were evidenced in the EPR results. A greater EPR intensity was observed by PHP compared to TNPP only, validating that PHP can generate more $^1O_2$ via energy transfer. To sum, the EPR results confirmed the coexistence of both reaction pathways of electron transfer (to produce superoxide anion radical $O_2^{\bullet-}$) and energy transfer (to produce singlet oxygen $^1O_2$) in the oxidative benzylamine coupling reactions.

The rates of the photocatalytic reaction of benzylamines and its para-substituted derivatives (X = OMe, H, Me and Cl groups) have been investigated using PHP and TNPP to obtain the Hammett plot (Fig. S25 and S26, ESI†). A linear relationship between $\log(k_x/k_h)$ values and Brown–Okamoto constant (σ_p^+) parameters[48] was fitted with a downward slope, thereby implying hole transfer from porphyrin π-cation radicals in PHP to the benzylamine substrate to give a positively charged intermediate (Fig. 3c). Based on the aforementioned results and the comparison between the cooperative effect of $O_2^{\bullet-}$ and $^1O_2$ in the reaction over PHP, it is concluded that $^1O_2$ is the sole ROS source. This behaviour accounts for the poor activity of TNPP as depicted in Table S2 (ESI†), entry 3. Moreover, the fact that there is no clear linearity correlation between $\log(k_x/k_h)$ and σ_p^+ in the Hammett plot (Fig. S26, ESI†) attests to the lack of positively charged intermediates, which are generated by the hole activation pathway by TNPP catalysts.

Control experiments suggested that only trace product was observed in the absence of either light or PHP as a photocatalyst, respectively (entries 2 and 3, Table S3, ESI†). Thus, to discern the assignments and the reaction mechanism of the photogenerated electron/hole pairs in the photochemical transformation of benzylamine to imine, further control experiments were undertaken. Practically, upon replacing O_2 with N_2 gas, we found that benzylamine was hardly transformed to the corresponding product (entry 4, Table S3, ESI†). This observation emphasizes the important role of oxygen in the reaction. However, the addition of potassium iodide (KI), as the hole scavenger, resulted in a lower conversion of 29% (entry 5, Table S3, ESI†). When adopting sodium azide as the singlet oxygen $^1O_2$ scavenger, a conversion of 64% was obtained (entry 6, Table S3, ESI†). The addition of P-benzoquinone (BQ), as an $O_2^{\bullet-}$ scavenger, under the same conditions, resulted in a low yield of the desired product (entry 7, Table S3, ESI†).

Based on these findings, it was concluded that the following three-in-one mechanisms are responsible for the remarkable photocatalytic activity of PHP (Fig. 3c). For the reductive pathway, photo-induced electrons in the CB level of PHP are strong reductants that are capable of capturing O_2 onto the surface and accordingly reducing it to $O_2^{\bullet-}$. Meanwhile, PHP$^+$ is generated during the photocatalytic cycles after the electron is transferred to oxygen. Spontaneously, the photo-generated holes on the PHP$^+$ oxidize the substrate BA to yield the benzylamine cation radical (BA$^{\bullet+}$). The porphyrin units in PHP can generate $^1O_2$ species under light irradiation via the triplet state. For the oxidative pathway, the BA$^{\bullet+}$ can be oxidized by both activated oxygen species, separately. Here, the $O_2^{\bullet-}$ radical first produces a highly reactive HO_2^- species that later oxidizes the BA$^{\bullet+}$ to the product. $^1O_2$ subsequently oxidizes the BA$^{\bullet+}$ to the product directly.

Taken together, the combined experimental and theoretical results support the preferred active sites in PHP for oxidative coupling reactions and the electron transfer pathway at the porphyrin and heptazine moieties, respectively. The incorporation of porphyrin molecules into the π-conjugated framework allows the separation of the reduction and oxidation sites as well as the modification of the electronic density of the porphyrin. Such a cooperative activation process benefits not only the energy transfer pathway but also the spatial charge separation, thus improving the photocatalytic process involved in the simultaneous reactions.

Conclusions

In summary, we report a novel porous porphyrin-heptazine polymer as a designed three-in-one photocatalyst for organic transformations. As evidenced by the mechanistic insight into thermodynamics and kinetics, the high photocatalytic efficiency reflects the synergistic effects on the electron transfer pathway (superoxide anion radical) and the energy transfer pathway (singlet oxygen). Furthermore, we demonstrated that the basic mechanism in this study is universal, and similar principles can be applied to create other porous organic polymer catalysts through a three-in-one approach. It is thus believed that these findings potentially provide new avenues towards more energy-efficient photocatalysts and related energy conversion systems.

Data availability

The data that support the findings of this study are available from the corresponding author upon reasonable request. This includes raw and processed data generated during the current study. Any additional data or materials required for replication of the results can also be provided by the corresponding author.

Conflicts of interest

There are no conflicts to declare.

Acknowledgements

Notes and references

1 A. Hagfeldt and M. Graetzel, *Chem. Rev.*, 2002, **95**, 49–68.

2 M. Gilbert and B. Albinsson, *Chem. Soc. Rev.*, 2015, **44**, 845–862.

3 P. Heremans, D. Cheyns and B. P. Rand, *Acc. Chem. Res.*, 2009, **42**, 1740–1747.

4 R. C. Coffin, J. Peet, J. Rogers and G. C. Bazan, *Nat. Chem.*, 2009, **1**, 657–661.

5 R. Neumann and M. Dahan, *Nature*, 1997, **388**, 353–355.

6 J.-S. M. Lee and A. I. Cooper, *Chem. Rev.*, 2020, **120**, 2171–2214.

7 X. Gao, C. Shu, C. Zhang, W. Ma, S.-B. Ren, F. Wang, Y. Chen, J. H. Zeng and J.-X. Jiang, *J. Mater. Chem. A*, 2020, **8**, 2404–2411.

8 K. Zhang, W. Liu, Y. Gao, X. Wang, Z. Chen, R. Ning, W. Yu, R. Li, L. Li, X. Li, K. Yuan, L. Ma, N. Li, C. Shen, W. Huang, K. Xie and K. P. Loh, *Adv. Mater.*, 2021, **33**, e2006323.

9 F. Lan, Q. Wang, H. Chen, Y. Chen, Y. Zhang, B. Huang, H. Liu, J. Liu and R. Li, *ACS Catal.*, 2020, **10**, 12976–12986.

10 L. Stegbauer, S. Zech, G. Savasci, T. Banerjee, F. Podjaski, K. Schwinghammer, C. Ochsenfeld and B. V. Lotsch, *Adv. Energy Mater.*, 2018, **8**, 1703278.

11 J. Wu, F. Xu, S. Li, P. Ma, X. Zhang, Q. Liu, R. Fu and D. Wu, *Adv. Mater.*, 2019, **31**, 1802922.

12 S. Lee, G. Barin, C. M. Ackerman, A. Muchenditsi, J. Xu, J. A. Reimer, S. Lutsenko, J. R. Long and C. J. Chang, *J. Am. Chem. Soc.*, 2016, **138**, 7603–7609.

13 Q. Sun, Z. Dai, X. Meng and F. S. Xiao, *Chem. Soc. Rev.*, 2015, **44**, 6018–6034.

14 Z. Xiang, R. Mercado, J. M. Huck, H. Wang, Z. Guo, W. Wang, D. Cao, M. Haranczyk and B. Smit, *J. Am. Chem. Soc.*, 2015, **137**, 13301–13307.

15 Y. Xu, S. Jin, H. Xu, A. Nagai and D. Jiang, *Chem. Soc. Rev.*, 2013, **42**, 8012–8031.

16 Y. Xie, T. T. Wang, X. H. Liu, K. Zou and W. Q. Deng, *Nat. Commun.*, 2013, **4**, 1960.

17 Y. L. Zhu, H. Long and W. Zhang, *Chem. Mater.*, 2013, **25**, 1630–1635.

18 G. Zhang, Z.-A. Lan and X. Wang, *Angew. Chem., Int. Ed.*, 2016, **55**, 15712–15727.

19 R. S. Sprick, J. X. Jiang, B. Bonillo, S. Ren, T. Ratvijitvech, P. Guiglion, M. A. Zwijnenburg, D. J. Adams and A. I. Cooper, *J. Am. Chem. Soc.*, 2015, **137**, 3265–3270.

20 J. Chun, S. Kang, N. Park, E. J. Park, X. Jin, K. D. Kim, H. O. Seo, S. M. Lee, H. J. Kim, W. H. Kwon, Y. K. Park, J. M. Kim, Y. D. Kim and S. U. Son, *J. Am. Chem. Soc.*, 2014, **136**, 6786–6789.

21 Z. A. Lan, G. Zhang, X. Chen, Y. Zhang, K. A. I. Zhang and X. Wang, *Angew. Chem., Int. Ed.*, 2019, **131**, 10342–10346.

22 Z. Mi, T. Zhou, W. Weng, J. Unruangsri, K. Hu, W. Yang, C. Wang, K. A. I. Zhang and J. Guo, *Angew. Chem., Int. Ed.*, 2021, **60**, 9642–9649.

23 W. Huang, N. Huber, S. Jiang, K. Landfester and K. A. I. Zhang, *Angew. Chem., Int. Ed.*, 2020, **59**, 18368–18373.

24 X. Wang, L. Chen, S. Y. Chong, M. A. Little, Y. Wu, W. H. Zhu, R. Clowes, Y. Yan, M. A. Zwijnenburg, R. S. Sprick and A. I. Cooper, *Nat. Chem.*, 2018, **10**, 1180–1189.

25 L. Wang, Y. Wan, Y. Ding, S. Wu, Y. Zhang, X. Zhang, G. Zhang, Y. Xiong, X. Wu, J. Yang and H. Xu, *Adv. Mater.*, 2017, **29**, 1702428.

26 Y. Xu, N. Mao, C. Zhang, X. Wang, J. Zeng, Y. Chen, F. Wang and J.-X. Jiang, *Appl. Catal., B*, 2018, **228**, 1–9.

27 L. Li, Z. Cai, Q. Wu, W. Y. Lo, N. Zhang, L. X. Chen and L. Yu, *J. Am. Chem. Soc.*, 2016, **138**, 7681–7686.

28 H. J. Son, S. Jin, S. Patwardhan, S. J. Wezenberg, N. C. Jeong, M. So, C. E. Wilmer, A. A. Sarjeant, G. C. Schatz, R. Q. Snurr, O. K. Farha, G. P. Wiederrecht and J. T. Hupp, *J. Am. Chem. Soc.*, 2013, **135**, 862–869.

29 X. Chen, M. Addicoat, E. Jin, L. Zhai, H. Xu, N. Huang, Z. Guo, L. Liu, S. Irle and D. Jiang, *J. Am. Chem. Soc.*, 2015, **137**, 3241–3247.

30 S. U. Raut, K. R. Balinge, S. A. Deshmukh, S. H. Barange, B. C. Mataghare and P. R. Bhagat, *Catal. Sci. Tech.*, 2022, **12**, 5917–5931.

31 S. U. Raut, S. A. Deshmukh, S. H. Barange and P. R. Bhagat, *Catal. Today*, 2023, **408**, 81–91.

32 S. U. Raut and P. R. Bhagat, *Fuel*, 2021, **303**, 121154.

33 S. Jin, M. Supur, M. Addicoat, K. Furukawa, L. Chen, T. Nakamura, S. Fukuzumi, S. Irle and D. Jiang, *J. Am. Chem. Soc.*, 2015, **137**, 7817–7827.

34 F. Su, S. C. Mathew, L. Mohlmann, M. Antonietti, X. Wang and S. Blechert, *Angew. Chem., Int. Ed.*, 2011, **50**, 657–660.

35 P. Arab, M. G. Rabbani, A. K. Sekizkardes, T. Islamoglu and H. M. El-Kaderi, *Chem. Mater.*, 2014, **26**, 1385–1392.

36 H. A. Patel, S. H. Je, J. Park, D. P. Chen, Y. Jung, C. T. Yavuz and A. Coskun, *Nat. Commun.*, 2013, **4**, 1357.

37 A. Atilgan, M. M. Cetin, J. Yu, Y. Beldjoudi, J. Liu, C. L. Stern, F. M. Cetin, T. Islamoglu, O. K. Farha, P. Deria, J. F. Stoddart and J. T. Hupp, *J. Am. Chem. Soc.*, 2020, **142**, 18554–18564.

38 M. Cao, R. Pang, Q. Y. Wang, Z. Han, Z. Y. Wang, X. Y. Dong, S. F. Li, S. Q. Zang and T. C. W. Mak, *J. Am. Chem. Soc.*, 2019, **141**, 14505–14509.

39 Y. Liu, S. Y. Moon, J. T. Hupp and O. K. Farha, *ACS Nano*, 2015, **9**, 12358–12364.

40 I. Fernandez and N. Khiar, *Chem. Rev.*, 2003, **103**, 3651–3705.

41 B. Chen, L. Wang and S. Gao, *ACS Catal.*, 2015, **5**, 5851–5876.

42 Z. J. Wang, S. Ghasimi, K. Landfester and K. A. Zhang, *Chem. Commun.*, 2014, **50**, 8177–8180.

43 P. M. Wood, *Biochem. J.*, 1988, **253**, 287–289.

44 Z. J. Wang, S. Ghasimi, K. Landfester and K. A. Zhang, *Adv. Mater.*, 2015, **27**, 6265–6270.

45 H. Q. Xu, J. Hu, D. Wang, Z. Li, Q. Zhang, Y. Luo, S. H. Yu and H. L. Jiang, *J. Am. Chem. Soc.*, 2015, **137**, 13440–13443.

46 J. H. Park, K. C. Ko, E. Kim, N. Park, J. H. Ko, D. H. Ryu, T. K. Ahn, J. Y. Lee and S. U. Son, *Org. Lett.*, 2012, **14**, 5502–5505.

47 J. Park, D. Feng, S. Yuan and H. C. Zhou, *Angew. Chem., Int. Ed.*, 2015, **54**, 430–435.

48 C. Xu, H. Liu, D. Li, J. H. Su and H. L. Jiang, *Chem. Sci.*, 2018, **9**, 3152–3158.